



THE UNIVERSITY *of* EDINBURGH

Edinburgh Research Explorer

## Flexible/Bendable Acoustofluidics Based on Thin Film Surface Acoustic Waves on Thin Aluminum Sheets

### Citation for published version:

wang, Y, Zhang, Q, Tao, R, Xie, J, Canyelles-Pericas, P, Torun, H, Reboud, J, McHale, G, Dodd, L, Yang, X, Luo, J, Wu, Q & Fu, Y 2021, 'Flexible/Bendable Acoustofluidics Based on Thin Film Surface Acoustic Waves on Thin Aluminum Sheets', *ACS Applied Materials & Interfaces*, vol. 13, no. 14, pp. 16978–16986. <https://doi.org/10.1021/acscami.0c22576>

### Digital Object Identifier (DOI):

[10.1021/acscami.0c22576](https://doi.org/10.1021/acscami.0c22576)

### Link:

[Link to publication record in Edinburgh Research Explorer](#)

### Document Version:

Peer reviewed version

### Published In:

ACS Applied Materials & Interfaces

### General rights

Copyright for the publications made accessible via the Edinburgh Research Explorer is retained by the author(s) and / or other copyright owners and it is a condition of accessing these publications that users recognise and abide by the legal requirements associated with these rights.

### Take down policy

The University of Edinburgh has made every reasonable effort to ensure that Edinburgh Research Explorer content complies with UK legislation. If you believe that the public display of this file breaches copyright please contact [openaccess@ed.ac.uk](mailto:openaccess@ed.ac.uk) providing details, and we will remove access to the work immediately and investigate your claim.



# Flexible/Bendable Acoustofluidics Based on Thin Film Surface Acoustic Waves on Thin Aluminum Sheets

Yong Wang<sup>a,b,c,†</sup>, Qian Zhang<sup>a,b,†</sup>, Ran Tao<sup>d,b</sup>, Jin Xie<sup>a,\*</sup>, Pep Canyelles-Pericas<sup>e</sup>, Hamdi Torun<sup>b</sup>,  
Julien Reboud<sup>f</sup>, Glen McHale<sup>g</sup>, Linzi E. Dodd<sup>b</sup>, Xin Yang<sup>h</sup>, Jingting Luo<sup>d</sup>, Qiang Wu<sup>b</sup>,  
and YongQing Fu<sup>b,\*</sup>

<sup>a</sup> The State Key Laboratory of Fluid Power and Mechatronic Systems, Zhejiang University, Hangzhou 310027, China

<sup>b</sup> Faculty of Engineering and Environment, University of Northumbria, Newcastle upon Tyne NE1 8ST, UK

<sup>c</sup> Key Laboratory of 3D Micro/Nano Fabrication and Characterization of Zhejiang Province, School of Engineering, Westlake University, Hangzhou 310024, China

<sup>d</sup> Shenzhen Key Laboratory of Advanced Thin Films and Applications, College of Physics and Optoelectronic Engineering, Shenzhen University 518060, China

<sup>e</sup> Department of Integrated Devices and Systems, MESA+ Institute, University of Twente, Enschede 7522NH, The Netherlands

<sup>f</sup> Division of Biomedical Engineering, James Watt School of Engineering, University of Glasgow, Glasgow G12 8LT, UK

<sup>g</sup> Institute for Multiscale Thermofluids, School of Engineering, University of Edinburgh, Kings Buildings, Edinburgh EH9 3FB, UK

<sup>h</sup> Department of Electrical and Electronic Engineering, School of Engineering, Cardiff University, Cardiff CF24 3AA, UK

<sup>†</sup> These authors contributed equally to this paper.

\* Corresponding authors: xiejin@zju.edu.cn; richard.fu@northumbria.ac.uk

## ABSTRACT

In this paper, we explore the acoustofluidic performance of zinc oxide (ZnO) thin film surface acoustic wave (SAW) devices fabricated on flexible and bendable thin aluminum (Al) foils/sheets with thicknesses from 50  $\mu\text{m}$  to 1500  $\mu\text{m}$ . Directional transport of fluids along these flexible/bendable surfaces offers potential applications for the next generation of microfluidic systems, wearable biosensors and soft robotic control. Theoretical calculations indicate that bending under strain levels up to 3000  $\mu\epsilon$  causes small frequency shift and amplitude change ( $< 0.3\%$ ) without degrading acoustofluidic performance. Through systematic investigation of the effects of Al sheet thickness on microfluidic actuation performance for the bent devices, we identify optimum thickness range to both maintain efficient microfluidic actuation and enable significant deformation of the substrate, providing a guide to design such devices. Finally, we demonstrate efficient liquid transportation across a wide range of substrate geometries including inclined, curved, vertical, inverted and lateral positioned surfaces using 200  $\mu\text{m}$  thick Al sheet SAW device.

**Keywords:** Acoustofluidics, Flexible devices, ZnO thin films, Surface acoustic waves, Aluminum sheets

## 1. Introduction

The ability to actuate liquids along flexible, deformed, three-dimensional (3D) complex surfaces is important for designs of flexible biomedical platforms for drug delivery, wearable biosensors, and lab-on-a-chip (LOC) diagnostic applications,<sup>1-4</sup> as well as smart microsystems such as those for soft robotic control.<sup>5,6</sup> They have shown superior advantages over rigid solutions for flexibility, deformability, structure compactness and conformability. Acoustic wave technologies, especially those based on piezoelectric thin films, have attracted great attention for microfluidic actuation and manipulation due to their advantages such as simple fabrication, remote and effective driving capability, and multi-functionality.<sup>7-9</sup> Using thin film SAW devices, such as those fabricated on ZnO or AlN films, various essential microfluidic functions can be achieved, including streaming,<sup>3</sup> concentration,<sup>10</sup> pumping,<sup>11</sup> mixing,<sup>12</sup> jetting and nebulization.<sup>13,14</sup>

However, most thin film acoustofluidic devices have been built on rigid substrates such as silicon and glass,<sup>13-15</sup> preventing their applications to those that require flexibility, deformability and integration within complex shapes and structures. In addition, many of these rigid substrates have limited efficiencies in enabling fluid transport on the device surface, due to the fact that forces acting on the liquid have a relatively small horizontal component (but a strong normal one). This can be measured by the Rayleigh angle (e.g., refraction angle into the liquid),  $\theta_R = \sin^{-1}(C_F/C_S)$ ,<sup>16,17</sup> where  $C_F$  is the sound speed in the liquid,  $C_S$  is the SAW propagation speed in the substrate. The phase velocities of Rayleigh waves on Si substrate and LiNbO<sub>3</sub> substrate are 4680 m/s and 3990 m/s,<sup>18,19</sup> respectively, thus generating the Rayleigh angles in water of  $\sim 22^\circ$  for LiNbO<sub>3</sub> based SAW device and  $\sim 21^\circ$  for ZnO/Si thin film SAW device ( $C_F$  for water = 1495 m/s).<sup>19,20</sup> Substrates with lower acoustic velocities (for example, aluminum has an acoustic speed of  $\sim 2888$  m/s and generates a Rayleigh angle of  $\sim 31.2^\circ$ ) are more attractive for fluid transport on its surface.<sup>21</sup>

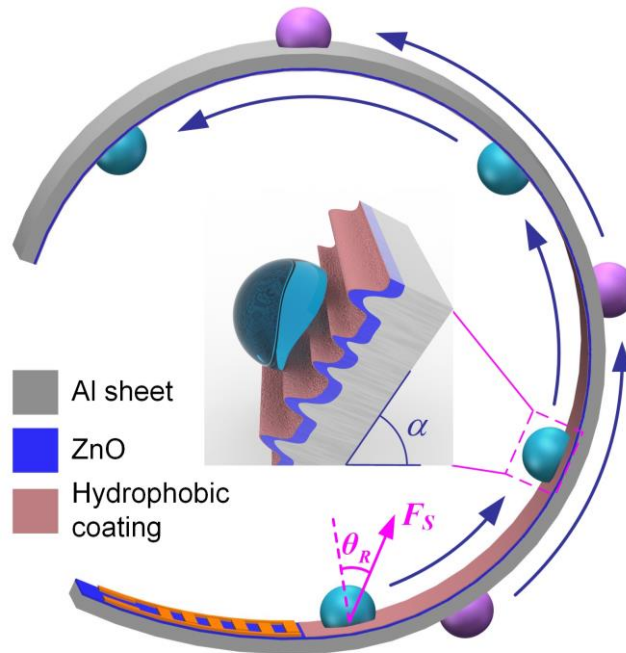


**Figure 1.** Schematic of droplet transportation along a curved surface using a flexible SAW device made with ZnO deposited on the Al sheet. A pseudo-Rayleigh or Lamb wave propagates along the sheet/foil, thereby enabling the actuation of the droplet on both sides of SAW device. The inset shows the droplet on the hierarchically textured surface with both slippery and sticky nature for efficient droplet transportation.

ZnO films deposited on Al sheets (including thin sheets and foils) exhibit low film stress, useful film adhesion and significantly reduced acoustic energy dissipation,<sup>22,23</sup> compared to other flexible substrates, such as polymers.<sup>24-26</sup> When

the Al sheets are of sub-millimeters in thickness, they can be easily bent or deformed, and then maintain their new shapes, or be further bent to other shapes or bent back to their original shapes (see Figure 1 for a simple illustration).<sup>27,28</sup> Moreover, as the Al sheets/foils are commonly fabricated with cold rolling manufacturing process, their surfaces have groove patterns with microscale roughness.<sup>29</sup> When the ZnO thin films are deposited onto their surfaces, a nanostructured morphology forms on top of this microscale roughness (see the inset in Figure 1).<sup>5</sup> If the ZnO/Al surface is further coated with a hydrophobic layer, a hierarchically textured and hydrophobic surface is generated, which is not only slippery (showing a low contact angle hysteresis and reducing the droplet pinning force) but also sticky (retaining an appropriate receding contact angle to ensure the droplet adhering to the inclined surface) for efficient liquid transportation on the deformable platform.

Thinner substrates are easier to bend, but this comes to the detrimental effect for acoustofluidic performance, as it becomes difficult to support efficient microfluidic actuation when the thickness of the Al foils is below 50 microns.<sup>30</sup> This is mainly due to their poor stiffness which causes a large deformation at a high RF power, thereby causing significant dissipation of acoustic energy into the substrate. Another major factor is the change of wave modes as the Rayleigh waves change into Lamb waves,<sup>22</sup> which is less efficient than Rayleigh waves for fluidic actuation.<sup>31</sup> Conversely, thick Al sheets (e.g., >1 mm) do not easily deform. We thus hypothesized that there should be an optimum thickness range (e.g., above 100 microns but below a millimeter) for efficient, yet flexible acoustofluidics.

In this paper, we aim to provide a guide for the design and manufacture of flexible, yet efficient acoustofluidic devices, by systematically investigating acoustofluidic behaviors of ZnO/Al sheet SAWs and comparing the performance with those of conventional ZnO/Si SAWs, focusing on thickness effects on wave modes and microfluidic performance. Theoretical calculations using a stiffness matrix method are presented to investigate the changes of acoustic wave velocities and amplitudes caused by the bending of the SAW devices. We demonstrate that thickness and deformability can be optimized for specific applications. In our example of Al sheets, a thickness of 200  $\mu\text{m}$  enables optimal fluid transportations along various mechanically bent/deformed surfaces, paving the way for flexible/bendable or wearable applications.

## 2. Materials and methods

ZnO films of  $\sim 5 \mu\text{m}$  thick were deposited onto commercially available Al foil/sheet substrates (with thicknesses of  $50 \pm 5 \mu\text{m}$ ,  $200 \pm 5 \mu\text{m}$ ,  $600 \pm 10 \mu\text{m}$  and  $1500 \mu\text{m} \pm 10 \mu\text{m}$ ) using DC magnetron sputtering processes. For the Al foils with thickness of  $50 \mu\text{m}$ , they were put on a bulk Al plate substrate to keep the flatness during the thin film deposition. The films were also deposited onto 4-inch silicon (100) wafer ( $500 \mu\text{m}$  thick) for comparisons. For the film deposition, a zinc target with a purity of 99.999% was used. ZnO films were deposited onto the above substrates using an Ar/O<sub>2</sub> gas flow rate of 10/13 sccm, a DC target power of 400 W and a chamber pressure of  $\sim 3$  mTorr. The distance between the zinc target and the sample holder was 70 mm. In addition, the sample holder was rotated to obtain uniform ZnO thin films. Crystal orientations of the deposited ZnO films were analyzed using X-ray diffraction (XRD, D5000, Siemens) with Cu-K $\alpha$  radiation ( $\lambda = 1.5406 \text{ \AA}$ ). Surface morphologies of ZnO films were observed using a scanning electron microscope (SEM, S-4100, Hitachi). SAW devices were fabricated on the prepared substrates by patterning Cr (20 nm)/Au (100 nm) film to form the interdigital transducer (IDT) electrodes using standard photolithography and lift-off processes. Each IDT was composed of 60 pairs of fingers, with a spatial periodicity of either  $64 \mu\text{m}$  or  $200 \mu\text{m}$ , and an acoustic aperture of 5 mm. The reflection spectra ( $S_{11}$ ) of the SAW devices were measured using an RF network analyzer (Agilent E5061B). The electromechanical coupling coefficients  $k^2$  of the SAW device were experimentally determined using the following equation derived from the Smith's equivalent model:<sup>32-34</sup>

$$k^2 = \frac{\pi}{4N} \left( \frac{G}{B} \right)_{f=f_0} \quad (1)$$

where  $N$  is the number of IDT finger pairs,  $G$  is the conductance (real part) and  $B$  is the susceptance (imaginary part) of the electrical admittance  $Y = G + jB$ , at the central frequency, respectively. The values of  $G$  and  $B$  can be obtained from the Smith Charts of the reflection coefficient ( $S_{11}$ ) at the central resonant frequency from a network analyzer.

The surfaces of the SAW devices were treated with a layer of ~200 nm thick fluoropolymer coating (CYTOP®, Asahi Glass Co., Tokyo, Japan) and heated to 120 °C for 10 min in order to make the device surface hydrophobic. A drop shape analyzer (Kruss DSA30S) was used to characterize the hysteresis resistance force of the droplet movement through measuring the advancing angle and receding angle.<sup>35</sup> The measured static contact angle, advancing angle, receding angle and contact angle hysteresis of the droplet (1  $\mu$ L) on the device surface are listed in Table S1 in the supporting information (SI). After the hydrophobic treatment, the contact angle hysteresis of the droplet (1  $\mu$ L) on the ZnO/Si surface was decreased from  $62.9^\circ \pm 8^\circ$  to  $27.2^\circ \pm 6^\circ$ . Whereas for the surface of ZnO/Al plate (1500  $\mu$ m thick), the contact angle hysteresis was decreased from  $25.1^\circ \pm 10^\circ$  to  $13.1^\circ \pm 5^\circ$ .

For microfluidic testing, the SAW devices were placed on top of an aluminum alloy test holder to minimize acoustic heating.<sup>36</sup> An RF input signal was generated using a signal generator (Marconi 2024) and amplified by a power amplifier (Amplifier research, 75A250) before being fed into the input IDTs. The input SAW power was measured using an RF power meter (Racal Instruments 9104). The microfluidic behaviors (including pumping and jetting) were observed using a standard video camera (60 fps) and a high-speed video camera (FASTCAM-ultima APX with a frame rate of 40000 fps). A photograph of the experimental setup for microfluidic test is shown in Figure S1 in the SI.

To understand wave vibration patterns on different thick Al sheets, finite element analysis (FEA) was performed using COMSOL Multiphysics (5.3a) with solid mechanics and electrostatics modules. A simplified two-dimensional (2D) model with ideal material parameters, one pair of IDT electrode and periodical boundary conditions were used to simulate the wave vibration patterns on different Al sheets. Moreover, a modified stiffness matrix method and elasto-plastic theory were implemented in MATLAB to analyze the frequency shifts and amplitude changes of the SAW device under different bending strains.<sup>37,38</sup> To simplify the calculation process, a pure bending condition, a zero residual stress and no cracks were assumed after the bending. The modelling and calculation details can be seen in the Methodology in the SI.

### 3. Results and discussion

#### 3.1. Film and device characterization

Figure 2a shows XRD spectra of ZnO thin films on different thick Al substrates. Results show that all the ZnO films on Al foils, Al sheets and Al plates have a dominant diffraction peak at  $2\theta$  of  $\sim 34.3^\circ$ , indicating a preferential growth orientation along the  $c$ -axis (0002).<sup>23</sup> Figure S2 in the SI shows the cross-section SEM image of ZnO films on Al foils, indicating the formation of columnar morphology of ZnO microstructure. The ZnO films deposited on Si substrate, which are used for comparison, also show a good  $c$ -axis (0002) orientation (see Figure S3 in the SI). Figure 2b shows the reflection spectra ( $S_{11}$ ) of the ZnO/Al plate (1500  $\mu$ m thick) SAW device with a wavelength of 64  $\mu$ m. For comparison, a ZnO/Si SAW device with the same electrode configuration was fabricated, with the reflection spectra ( $S_{11}$ ) shown in Figure S4 in the SI. The SAW propagation speed in ZnO thin film (2700 m/s) is smaller than those on Al plate ( $\sim 2888$  m/s) and Si (4680 m/s) substrates, thus generating both the Rayleigh mode ( $R_0$ ) and Sezawa mode.<sup>17,18</sup>

Figure 2c-f show the effects of Al sheet thickness (from 50  $\mu$ m to 1500  $\mu$ m) on wave modes when the device wavelength is 200  $\mu$ m. The thickness/wavelength ratio plays an important role in wave mode selection. When this ratio is much larger than one, Rayleigh waves are dominant. On the contrary, if the ratio is smaller than one, Lamb waves are dominant, whilst hybrid modes (both Rayleigh and Lamb waves) are commonly observed for a ratio near one.<sup>22</sup> The FEA simulation results for wave vibration patterns on different Al sheets show that when the Al sheet thickness (i.e., 600  $\mu$ m and 1500  $\mu$ m) is larger than the device wavelength, the SAW devices generate a Rayleigh mode and a Sezawa mode, as

depicted in Figure 2c,d. When the Al sheet thickness is in a similar range with the device wavelength,  $A_0$  mode and pseudo-Rayleigh mode are hybridized together at a frequency of 13.72 MHz, and the pseudo- $S_0$  mode and Sezawa mode are also obtained, as illustrated in Figure 2e. When Al sheet thickness is further decreased to 50  $\mu\text{m}$ , the wave vibration modes are changed into the typical Lamb waves, without Rayleigh and Sezawa modes observed, as shown in Figure 2f. The simulated wave modes for SAW devices with the wavelengths of 64  $\mu\text{m}$  and 200  $\mu\text{m}$  and Al sheet thicknesses from 50  $\mu\text{m}$  to 1500  $\mu\text{m}$  are shown in Figure S5 in the SI.

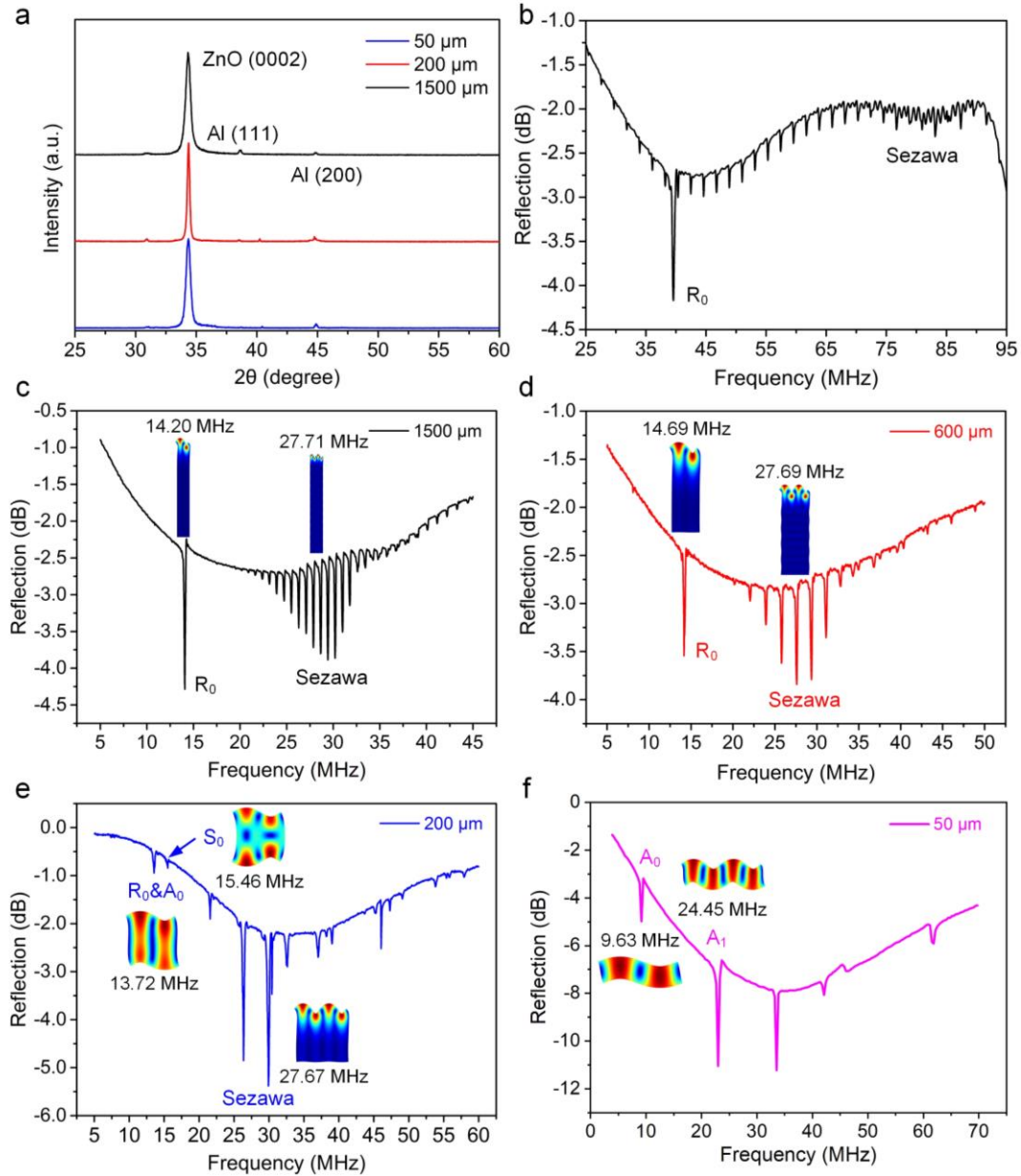


**Figure 2.** (a) XRD patterns of ZnO thin films on various thick Al sheet substrates. (b) Signal reflection spectra ( $S_{11}$ ) of ZnO/Al plate (1500  $\mu\text{m}$  thick) SAW device with the wavelength of 64  $\mu\text{m}$ . FEA simulation and experimental verification of wave vibration modes and their corresponding resonant frequencies for the SAW devices with 200  $\mu\text{m}$  wavelength and varied Al sheet thicknesses of (c) 1500  $\mu\text{m}$ , (d) 600  $\mu\text{m}$ , (e) 200  $\mu\text{m}$  and (f) 50  $\mu\text{m}$ .

### 3.2. Bending effects on device's frequency and amplitude

For flexible acoustofluidics applications, the SAW devices are often bent into different shapes. Therefore, we further studied the effects of bending on device's resonant frequency and acoustic wave amplitude. Here, a modified stiffness

matrix method was used for modelling and calculation.<sup>37</sup> For the modelling, the Al sheet thickness is set as 200  $\mu\text{m}$ , and the thickness of ZnO thin film is 5  $\mu\text{m}$ . A mechanical strain  $st/2r$  is defined as the strain on the ZnO surface, where  $t$  is the thickness of device,  $r$  is the curvature radius. For a tensile strain,  $s$  is selected as 1, and for a compressive strain,  $s$  is -1. When the SAW device is bent, all the densities and elastic constants of ZnO and Al as well as the device wavelengths will change. The total frequency shifts can be regarded as the sum of several frequency shift components caused by the changes of the density, elastic constant, device wavelength and the stress, respectively.<sup>39</sup>

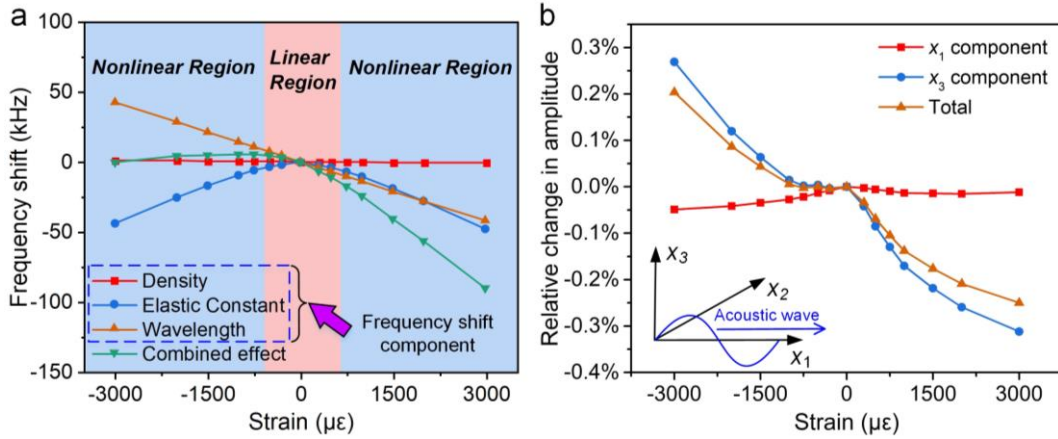


**Figure 3.** (a) The calculated contribution components of density, elastic constant, device wavelength changes under different bending strains to device's frequency shifts (taking the  $A_0$  mode for example). (b) Theoretically calculated relative acoustic wave amplitude changes (taking the  $A_0$  mode for example) on top surface of 200  $\mu\text{m}$  thick Al sheet device under different bending strains. The  $x_1$  and  $x_3$  components are the wave vibration components in the  $x_1$  (along the wave propagation) and  $x_3$  (perpendicular to the substrate surface) directions.

Figure 3a shows the calculated frequency shifts ( $A_0$  mode) due to the changes of density, elastic constant, and device's wavelength as function of bending strains. The frequency shift caused by the density change is relatively small ( $< 1\text{kHz}$  under strain levels of 3000  $\mu\epsilon$ ), whilst the change in elastic constant has a larger impact than that of the wavelength, leading to an apparent non-linear effect with the increase of strain. Nevertheless, for flexible acoustofluidic testing, a bending curvature of 50~100  $\text{m}^{-1}$  can be considered for most applications, which lead to calculated strains of -2750  $\mu\epsilon$  to -1375  $\mu\epsilon$ , corresponding to frequency shifts of about 1.2 to 5.1 kHz. Here, the positive strain represents the bending outward, while the negative strain is generated by the bending inward. With such a small frequency shift, the acoustic wave speed change is smaller than 0.3%. Before each acoustofluidics test, we have bent the SAW device into a new shape and maintained this shape, and its resonant frequency was measured using a network analyzer. Then the measured frequency value was input into the signal generator to excite the acoustic wave for microfluidic actuation.

As the acoustic wave amplitude determines the SAW driving force, the relative changes in acoustic wave amplitude ( $A_0$  mode) after the bending were further calculated, and the obtained results are shown in Figure 3b. Here, direction  $x_1$  is defined as that along the acoustic wave propagation direction (longitudinal component), while direction  $x_3$  is defined as that perpendicular to the substrate surface (transverse or shear vertical component).<sup>40</sup> When a positive strain is applied to the SAW device, the amplitude of  $x_1$  and  $x_3$  components both decrease with the strain. With the application of a negative strain, the  $x_1$  component decreases while the  $x_3$  component increases with the increase of strain values. For the bending strains considered previously (from -2750  $\mu\epsilon$  to -1375  $\mu\epsilon$ , or curvature from 50 to 100  $\text{m}^{-1}$ ), the relative changes in acoustic wave amplitude are less than 0.3%, indicating that the bending only has a limited influence on the acoustic wave amplitude. We have also demonstrated in experiment that when the thin Al sheet substrate (200  $\mu\text{m}$  thick) is bent to nearly 90° with a

curvature of  $\sim 50 \text{ m}^{-1}$ , the pseudo-Rayleigh or  $A_0$  mode the SAW device still carries a strong signal (see Figure S6 in the SI), thereby enabling an efficient microfluidic actuation on the flexible surfaces.

### 3.3. Acoustofluidic demonstration using ZnO/Al plate SAW device

As a baseline, we first chose the  $1500 \text{ }\mu\text{m}$  thick Al plate SAW device and investigated its microfluidic actuation behaviors along flat and inclined surfaces and compared them with those of well-studied and conventional ZnO/Si SAW devices.<sup>41</sup> Since the device wavelength has a significant effect on microfluidic performance, for these comparisons, we chose the SAW devices with the same wavelength of  $64 \text{ }\mu\text{m}$ . When a droplet is placed on the surface and maintained horizontally, the droplet movement on the Al plate surface is a combination of rolling and sliding (see the captured images shown in Figure S7a). Whereas for the ZnO/Si SAW device, the droplet movement on the surface is dominated by sliding and jumping (see the pumping images shown in Figure S7b). This is due to the lower acoustic velocity of the ZnO/Al plate SAWs compared to ZnO/Si SAWs, thereby generating a larger Rayleigh angle ( $31.2^\circ$  compared with  $20.9^\circ$ ), resulting in a larger horizontal component of the SAW driving force and consequently a more significant horizontal deformation (as evidenced in Figure S7).

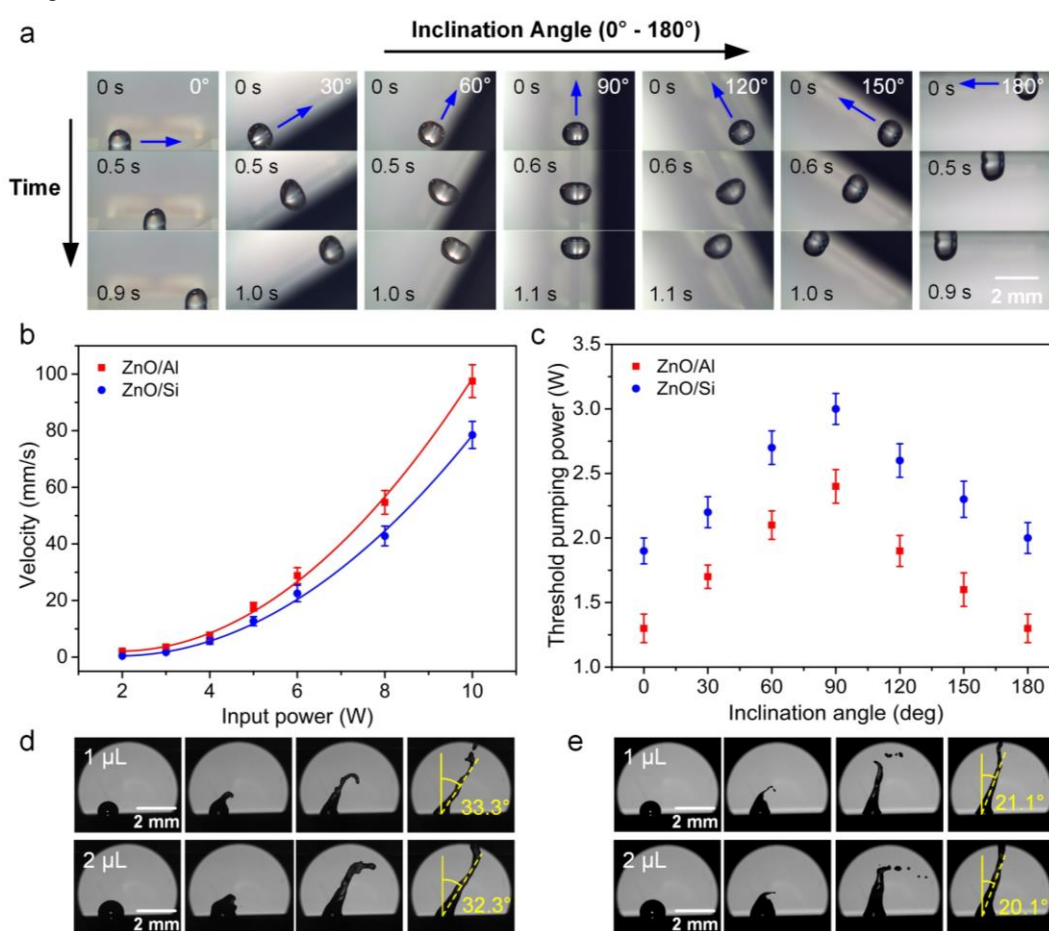


**Figure 4.** (a) Droplet ( $1 \text{ }\mu\text{L}$ ) pumping images along inclined surfaces with inclination angles from  $0^\circ$  to  $180^\circ$  using ZnO/Al plate SAW device with an input power of  $5 \text{ W}$ . (b) Comparisons of average pumping velocities for the droplet on the flat surface under different input powers between ZnO/Al plate SAW device and ZnO/Si SAW device. (c) Threshold powers of pumping a  $1 \text{ }\mu\text{L}$  droplet for ZnO/Al plate SAW device and ZnO/Si SAW device under different inclination angles. High-speed images indicating the jetting angles using (d) ZnO/Al plate SAW device and (e) ZnO/Si SAW device with the same input power of  $18 \text{ W}$ .

We further investigated microfluidic pumping characteristics when the surface is inclined with an angle  $\alpha$  (defined as the angle which the device substrate was tilted along the horizontal plane, as shown in Figure 1). Here, the droplet size and gravity play important roles, and when the droplet size is above a certain value, it slides down (Movie S1) or drops from the device surface.<sup>42,43</sup> This threshold decreased with increased inclination angle when the inclination angle is smaller than 90°, and increased with inclination angles increasing from 90° to 180°, as shown in Figure S8 in the SI. We have found that at the inclination angle of 90° (i.e., vertical alignment), the maximum droplet volume which can be pumped uphill shows its smallest value ( $\sim 3 \mu\text{L}$ ) compared with those at the other inclination angles, because the gravity component along the inclined surface reaches the maximum value. Figure 4a demonstrates that when the droplet volume is 1  $\mu\text{L}$ , it can be efficiently pumped along arbitrary inclined surfaces.

Figure 4b,c compare the pumping performance between ZnO/Al plate SAW device and ZnO/Si SAW device with the same wavelength of 64  $\mu\text{m}$ . Clearly, for both these SAW devices, the average pumping velocity for the droplet on the horizontal surface is increased with the increase of input power. At the same power, the droplet average pumping velocity using the ZnO/Al plate device is larger than that of the ZnO/Si SAW device, as shown in Figure 4b. Besides, ZnO/Al plate SAW device also requires a lower threshold power for microfluidic actuation when compared to that of ZnO/Si SAW device at the same inclination angle (e.g.,  $\sim 1.3 \text{ W}$  for the ZnO/Al plate SAWs and  $\sim 2.0 \text{ W}$  for the ZnO/Si SAWs for the horizontal surface). This threshold actuation/pumping power is defined as the minimum power to initiate the droplet movement, and a lower threshold power means that a smaller input power is needed to actuate the droplet. Therefore, in comparisons with the ZnO/Si SAW device, the ZnO/Al plate SAW device provides a better microfluidic actuation performance.

In addition to the increased Rayleigh angle as previously mentioned, the enhanced microfluidic actuation performance can also be attributed to a higher electromechanical coupling coefficient of ZnO/Al plate (1.57%) SAWs than that of ZnO/Si SAWs (1.08%), which enables more applied power to be transformed into acoustic energy given the same input power, thereby improving the energy efficiency. Moreover, the formation of a hierarchically textured surface on Al substrates generates a lower contact angle hysteresis, which then reduces the threshold actuation power.<sup>5</sup>

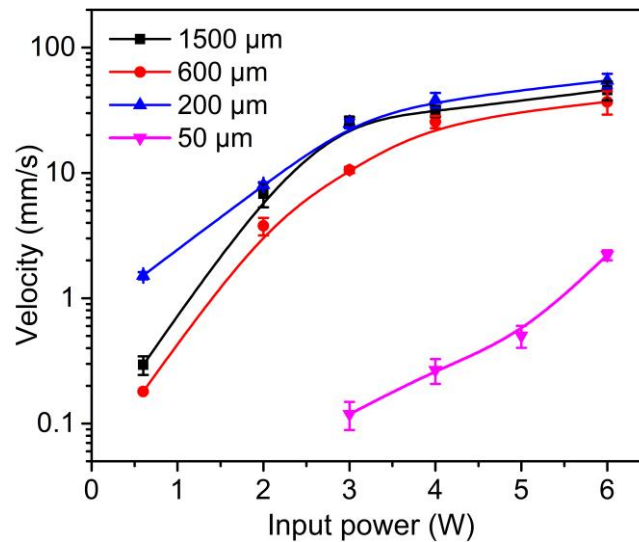
The Rayleigh angles can be further confirmed when performing jetting of the droplets at higher powers (see Figure S9 in the SI). After about 4 ms of actuation, a coherent liquid beam became dominant. The droplet jetting angles were measured as 33° for the ZnO/Al plate SAW device and 21° for the ZnO/Si SAW device, approximately following the Rayleigh angles of the corresponding SAW devices, as shown in Figure 4d,e.

### 3.4. Optimization of Al sheet thickness for acoustofluidics

To provide a guide for the design of flexible acoustofluidics devices, we systematically investigated the effects of Al sheet thickness on microfluidic actuation performance, using a SAW device with wavelength of 200  $\mu\text{m}$ . Table 1 summarizes threshold powers for pumping/jetting of a 1  $\mu\text{L}$  droplet for the SAW devices with different Al sheet thicknesses using different wave modes. Results show that for the 50  $\mu\text{m}$  thick Al foil SAW device, much higher powers are needed to transport the droplet compared to those of thicker Al substrate SAWs. The pumping performance of the  $A_0$  mode is better than that of the  $S_0$  mode and no droplet jetting were observed for any of the Lamb waves. The three types of thicker Al sheet SAW devices show comparable threshold pumping and jetting powers when using either Rayleigh or hybrid modes. No droplet jetting was observed when using Sezawa modes, mainly due to the fact that these are guided waves which propagate along the interface between the piezoelectric layer and the substrate, thus are less dissipating energy into surface droplet. In addition, the droplet jetting phenomena using Lamb wave modes (e.g.,  $A_0$  or  $S_0$  modes) of 200  $\mu\text{m}$  thick Al sheet SAW device have been observed (Movies S2 and S3).

Table 1. Threshold powers for pumping/jetting of a 1  $\mu\text{L}$  droplet for the SAW devices on different thick Al sheets with the same wavelength of 200  $\mu\text{m}$  using different wave modes.

Al sheet thickness ( $\mu\text{m}$ )		50	200	600	1500
Threshold pumping power (W)	$R_0$	—	0.5	0.6	0.5
	$A_0$	2.6	0.5	—	—
	$S_0$	7.0	2.1	—	—
	Sezawa	—	16	14	16
Threshold jetting power (W)	$R_0$	—	16	18	16
	$A_0$	—	16	—	—
	$S_0$	—	22	—	—
	Sezawa	—	—	—	—



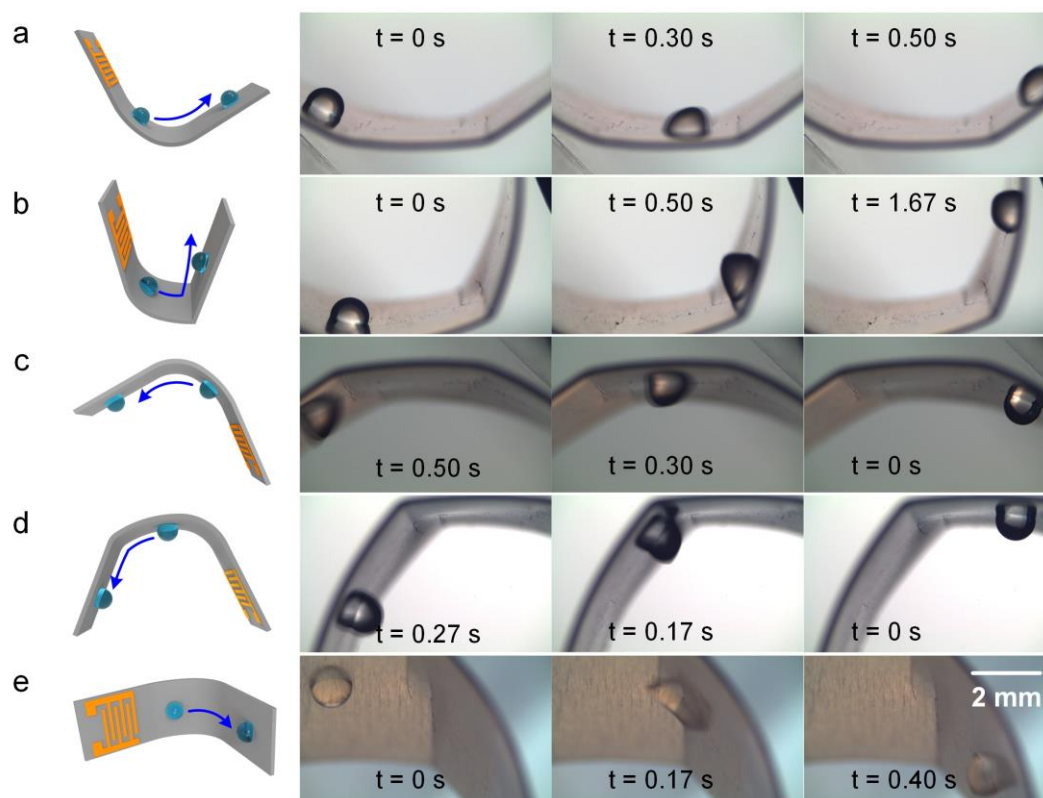
**Figure 5.** Droplet (1  $\mu\text{L}$ ) average pumping velocities as a function of input power, for thick Al plate (i.e., 600  $\mu\text{m}$  and 1500  $\mu\text{m}$ ) SAW devices driven using the Rayleigh mode, for thin Al sheet (200  $\mu\text{m}$  thick) and Al foil (50  $\mu\text{m}$  thick) SAW devices driven using pseudo- $R_0$  or  $A_0$  mode.

Figure 5 shows the average pumping velocities of a 1  $\mu\text{L}$  droplet for the SAW devices with different Al sheet thicknesses using the Rayleigh mode or the  $A_0$  mode with input powers varying from 0.6 W to 6 W. At the same input power, the 50  $\mu\text{m}$  thick Al foil SAW device shows the lowest droplet pumping velocity, consistent with its flexural wave mode, which does not transfer much energy into the liquid. The other reasons include the large deformation of the substrate (Movies S4 and S5), the increased acoustic dissipation, thus the reduced microfluidic driving efficiency. Therefore, although the Al foil-based SAW devices have relatively good flexibility, they do not exhibit the best microfluidic actuation performance. The 200  $\mu\text{m}$  thick Al sheet SAW device supports hybrid modes (e.g., pseudo-Rayleigh and Lamb waves at the same frequency, Figure 2e) with comparable pumping performance to those of 600  $\mu\text{m}$  and 1500  $\mu\text{m}$  thick Al plate SAW devices using the Rayleigh mode, making them highly suitable for application of flexible/bendable acoustofluidics.

In addition, the increase of ZnO thin film thickness might further enhance the microfluidic actuation performance on these flexible surfaces, due to its piezoelectric nature.

### 3.5. Demonstrations of acoustofluidics on flexible/bendable substrate: the 200 $\mu\text{m}$ case

To demonstrate the range of applications that could be achieved with the optimum 200  $\mu\text{m}$  thick Al sheet SAW device, it was deformed into different shapes and tilted to different orientations. Figure 6a,b show that the droplet can be efficiently transported on the bent surfaces with curvatures varying from 50 to 100  $\text{m}^{-1}$  (see Movie S6), which is corresponding to a nearly “U”-shaped path. We have also tilted the bent SAW device to different angles and demonstrated efficient transportation of the droplet on different spatial positions (e.g., inverted and downward), as shown in Figure 6c,d. For the inverted surface, the maximum droplet volume which can be pumped is about 7  $\mu\text{L}$  (Movie S7), otherwise the droplet would drop down from the surface. Figure 6e demonstrates the pumping/transportation of the droplet along the laterally bent surface. Therefore, in theory, when the droplet size is smaller than a certain value (here  $\leq 3 \mu\text{L}$ ), they can be efficiently transported on arbitrarily shaped and positioned surfaces using this SAW device (including on the backside, Movie S8, although at a slower speed). Otherwise, gravity of the droplet will become dominantly influenced. Furthermore, during the entire bending process, no distinct deterioration of the microfluidic actuation performance was observed, indicating a great potential of thin Al sheet SAWs for flexible/bendable acoustofluidics.



**Figure 6.** Demonstration of droplet pumping/transportation using ZnO thin film SAWs on the bent Al sheet (200  $\mu\text{m}$  thick) substrates. (a, b) 1  $\mu\text{L}$  droplet transportation along different bending curvature surfaces. (c, d) 1  $\mu\text{L}$  droplet transportation along different spatial position surfaces (e.g., inverted and downward). (e) 1  $\mu\text{L}$  droplet transportation along the laterally bent surface. The input SAW powers are 16 W.

## 4. Conclusions

In summary, through both systematic numerical and experimental characterization of the acoustofluidic behaviors of ZnO thin film SAW devices fabricated on different thick Al sheets, we provide the evidence of optimum conditions for acoustofluidics functionalities on bendable and deformable surfaces. We have demonstrated better microfluidic actuation performance of the ZnO/Al plate SAW device when compared to that of conventional ZnO/Si SAW device and verified efficient transportation of droplets along various inclined surfaces using these SAW devices. As the thickness is decreased, the wave vibration modes are changed from Rayleigh to hybrid modes and subsequently to Lamb waves. We have shown that in this specific study, 200  $\mu\text{m}$  is the optimal thickness to combine deformability and acoustofluidic actuation, enabling fluidic functions to be performed on complex 3D shapes. Our work proposes a new platform for flexible Al sheet SAW devices to perform versatile microfluidics, sensing and diagnostic applications.

## **Associated Content**

### *Supporting Information*

Contact angle hysteresis measurements on different device surfaces; Photograph of experimental setup for microfluidic test; Cross-section SEM image of the ZnO films on Al foils; XRD pattern of ZnO films on silicon substrate; Reflection spectra of ZnO/Si SAW device; FEA simulations of wave vibration modes for the SAW devices with different Al sheet thicknesses; Reflection spectra of thin Al sheet (200  $\mu\text{m}$  thick) SAW device before and after the bending; High-speed droplet pumping images using ZnO/Al plate and ZnO/Si SAW devices; Maximum droplet pumping volume under different inclination angles, High-speed droplet jetting images using ZnO/Al plate and ZnO/Si SAW devices (PDF)

Movie S1: 10  $\mu\text{L}$  droplet transport on 30° inclined surface using ZnO/Al plate SAW device with an actuation frequency of 39.63 MHz and an input power of 7 W (AVI)

Movie S2: 1  $\mu\text{L}$  droplet jetting using pseudo-Rayleigh or  $A_0$  mode of 200  $\mu\text{m}$  thick Al sheet SAW device with an actuation frequency of 13.58 MHz and an input power of 18 W (AVI)

Movie S3: 1  $\mu\text{L}$  droplet jetting using  $S_0$  mode of 200  $\mu\text{m}$  thick Al sheet SAW device with an actuation frequency of 15.56 MHz and an input power of 24 W (AVI)

Movie S4: 1  $\mu\text{L}$  droplet movement on the Al foil substrate driving using  $A_0$  mode of 50  $\mu\text{m}$ -thick Al foil SAW device with an actuation frequency of 9.38 MHz and an input power of 6 W (AVI)

Movie S5: 1  $\mu\text{L}$  droplet movement on the Al foil substrate driving using  $S_0$  mode of 50  $\mu\text{m}$ -thick Al foil SAW device with an actuation frequency of 25.1 MHz and an input power of 6 W (AVI)

Movie S6: 1  $\mu\text{L}$  droplet transport on the bent surface using the pseudo-Rayleigh or  $A_0$  mode of 200  $\mu\text{m}$  thick Al sheet SAWs with an actuation frequency 13.57 MHz and an input power of 16 W (AVI)

Movie S7: 6  $\mu\text{L}$  droplet transport on the inverted surface using the pseudo-Rayleigh mode of 200  $\mu\text{m}$  thick Al sheet SAWs with an actuation frequency 13.57 MHz and an input power of 16 W (AVI)

Movie S8: 1  $\mu\text{L}$  droplet transport on the backside of the 200  $\mu\text{m}$  thick Al sheet SAW device using the pseudo-Rayleigh mode with an input power of 5 W (AVI)

Methodology: Model; Assumption; Equation (PDF)

## **Notes**

The authors declare no competing financial interest.

## **Acknowledgements**

This work was supported by the Zhejiang Provincial Natural Science Foundation of China (LZ19E050002), the National Natural Science Foundation of China (51875521, 51605485 and 51575487), the UK Engineering and Physical Sciences Research Council (EPSRC EP/P018998/1 and UK Fluidic Network (EP/N032861/1)-Special Interest Group in Acoustofluidics), and Newton Mobility Grant (IE161019) through Royal Society and NFSC.

## References

- [1] Park, C.; Kim, H. R.; Kim, S. K.; Jeong, I. K.; Pyun, J. C.; Park, S. Three-Dimensional Paper-Based Microfluidic Analytical Devices Integrated with a Plasma Separation Membrane for the Detection of Biomarkers in Whole Blood. *ACS Appl. Mater. Interfaces* **2019**, *11*, 36428-36434.
- [2] Li, S.; Ma, Z.; Cao, Z.; Pan, L.; Shi, Y. Advanced Wearable Microfluidic Sensors for Healthcare Monitoring. *Small* **2020**, *16*, 1903822.
- [3] Tao, R.; Reboud, J.; Torun, H.; McHale, G.; Dodd, L. E.; Wu, Q.; Tao, K.; Yang, X.; Luo, J. T.; Todryk, S.; Fu, Y. Integrating Microfluidics and Biosensing on a Single Flexible Acoustic Device Using Hybrid Modes. *Lab Chip* **2020**, *20*, 1002-1011.
- [4] Abdelgawad, M.; Freire, S. L.; Yang, H.; Wheeler, A. R. All-terrain droplet actuation. *Lab Chip* **2008**, *8*, 672-677.
- [5] Tao, R.; McHale, G.; Reboud, J.; Cooper, J. M.; Torun, H.; Luo, J. T.; Luo, J.; Yang, X.; Zhou, J.; Canelles-Pericas, P.; Wu, Q.; Fu, Y. Hierarchical Nanotexturing Enables Acoustofluidics on Slippery yet Sticky, Flexible Surfaces. *Nano Lett.* **2020**, *20*, 3263-3270.
- [6] Yeo, J. C.; Lim, C. T. Emergence of microfluidic wearable technologies. *Lab Chip* **2016**, *16*, 4082-4090.
- [7] Friend, J.; Yeo, L. Y. Microscale Acoustofluidics: Microfluidics Driven via Acoustics and Ultrasonics. *Rev. Mod. Phys.* **2011**, *83*, 647-704.
- [8] Fu, Y. Q.; Luo, J. K.; Nguyen, N. T.; Walton, A. J.; Flewitt, A. J.; Zu, X. T.; Li, Y.; McHale, G.; Matthews, A.; Iborra, E.; Du, H.; Milne, W. I. Advances in Piezoelectric Thin Films for Acoustic Biosensors, Acoustofluidics and Lab-on-Chip Applications. *Prog. Mater. Sci.* **2017**, *89*, 31-91.
- [9] Ding, X.; Li, P.; Lin, S. C. S.; Stratton, Z. S.; Nama, N.; Guo, F.; Slotcavage, D.; Mao, X.; Shi, J.; Costanzo, F.; Huang, T. J. Surface Acoustic Wave Microfluidics. *Lab Chip* **2013**, *13*, 3626-3649.
- [10] Zhou, J.; Pang, H. F.; Garcia-Gancedo, L.; Iborra, E.; Clement, M.; De Miguel-Ramos, M.; Jin, H.; Luo, J. K.; Smith, S.; Dong, S. R.; Wang, D. M.; Fu, Y. Q. Discrete Microfluidics Based on Aluminum Nitride Surface Acoustic Wave Devices. *Microfluid. Nanofluid.* **2015**, *18*, 537-548.
- [11] Wang, Y.; Tao, X.; Tao, R.; Zhou, J.; Zhang, Q.; Chen, D.; Jin, H.; Dong, S.; Xie, J.; Fu, Y. Q. Acoustofluidics along Inclined Surfaces Based on AlN/Si Rayleigh Surface Acoustic Waves. *Sensors Actuators A* **2020**, *306*, 111967.
- [12] Wang, Y.; Tao, R.; Zhang, Q.; Chen, D.; Yang, L.; Huang, W.; Xie, J.; Fu, Y. Acoustofluidics Based on ZnO/Al Plate Surface Acoustic Wave Devices with Enhanced Performances. *Proc. IEEE Int. Conf. Micro Electro Mech. Syst.* **2020**, 38-41.
- [13] Pang, H. F.; Fu, Y. Q.; Garcia-Gancedo, L.; Porro, S.; Luo, J. K.; Placido, F.; Wilson, J. I. B.; Flewitt, A. J.; Milne, W. I.; Zu, X. T. Enhancement of Microfluidic Efficiency with Nanocrystalline Diamond Interlayer in the ZnO-Based Surface Acoustic Wave Device. *Microfluid. Nanofluid.* **2013**, *15*, 377-386.
- [14] Zhou, J.; Tao, X.; Luo, J.; Li, Y.; Jin, H.; Dong, S.; Luo, J. K.; Duan, H.; Fu, Y. Nebulization Using ZnO/Si Surface Acoustic Wave Devices with Focused Interdigitated Transducers. *Surf. Coatings Technol.* **2019**, *367*, 127-134.
- [15] Wang, W.; He, X.; Zhou, J.; Gu, H.; Xuan, W.; Chen, J.; Wang, X.; Luo, J. K. Comparative Study on Microfluidic Performance of ZnO Surface Acoustic Wave Devices on Various Substrates. *J. Electrochem. Soc.* **2014**, *161*, B230-B236.
- [16] Shiokawa, S.; Matsui, Y.; Ueda, T. Study on SAW Streaming and Its Application to Fluid Devices. *Jpn. J. Appl. Phys.* **1990**, *29*, 137-139.

- [17] Fu, Y. Q.; Luo, J. K.; Du, X. Y.; Flewitt, A. J.; Li, Y.; Markx, G. H.; Walton, A. J.; Milne, W. I. Recent Developments on ZnO Films for Acoustic Wave Based Bio-Sensing and Microfluidic Applications: A Review. *Sensors Actuators B* **2010**, *143*, 606-619.
- [18] Du, X. Y.; Fu, Y. Q.; Tan, S. C.; Luo, J. K.; Flewitt, A. J.; Milne, W. I.; Lee, D. S.; Park, N. M.; Park, J.; Choi, Y. J.; Kim, S. H.; Maeng, S. ZnO Film Thickness Effect on Surface Acoustic Wave Modes and Acoustic Streaming. *Appl. Phys. Lett.* **2008**, *93*, 094105.
- [19] Li, J.; Xu, N.; Dong, L.; Li, J.; Biroun, M. H.; Tao, R.; Torun, H.; Xu, N.; Rahmati, M.; Li, Y.; Fu, Y.; Tao, R.; Fu, C.; Luo, J.; Wang, Y.; Xie, J.; Gibson, D. Wide Range of Droplet Jetting Angles by Thin-Film Based Surface Acoustic Waves. *J. Phys. D: Appl. Phys.* **2020**, *53*, 355402.
- [20] Connacher, W.; Orosco, J.; Friend, J. Droplet Ejection at Controlled Angles via Acoustofluidic Jetting. *Phys. Rev. Lett.* **2020**, *125*, 184504.
- [21] McKie, A. D. W.; Wagner, J. W.; Spicer, J. B.; Deaton, J. B. Dual-Beam Interferometer for the Accurate Determination of Surface-Wave Velocity. *Appl. Opt.* **1991**, *30*, 4034-4039.
- [22] Tao, R.; Wang, W. B.; Luo, J. T.; Ahmad Hasan, S.; Torun, H.; Canyelles-Pericas, P.; Zhou, J.; Xuan, W. P.; Cooke, M. D.; Gibson, D.; Wu, Q.; Ng, W. P.; Luo, J. K.; Fu, Y. Q. Thin Film Flexible/Bendable Acoustic Wave Devices: Evolution, Hybridization and Decoupling of Multiple Acoustic Wave Modes. *Surf. Coatings Technol.* **2019**, *357*, 587-594.
- [23] Liu, Y.; Luo, J. T.; Zhao, C.; Zhou, J.; Hasan, S. A.; Li, Y.; Cooke, M.; Wu, Q.; Ng, W. P.; Du, J. F.; Yu, Q.; Liu, Y.; Fu, Y. Q. Annealing Effect on Structural, Functional, and Device Properties of Flexible ZnO Acoustic Wave Sensors Based on Commercially Available Al Foil. *IEEE Trans. Electron Devices* **2016**, *63*, 4535-4541.
- [24] Xuan, W.; He, X.; Chen, J.; Wang, W.; Wang, X.; Xu, Y.; Xu, Z.; Fu, Y. Q.; Luo, J. K. High Sensitivity Flexible Lamb-Wave Humidity Sensors with a Graphene Oxide Sensing Layer. *Nanoscale* **2015**, *7*, 7430-7436.
- [25] He, X. L.; Li, D. J.; Zhou, J.; Wang, W. B.; Xuan, W. P.; Dong, S. R.; Jin, H.; Luo, J. K. High Sensitivity Humidity Sensors Using Flexible Surface Acoustic Wave Devices Made on Nanocrystalline ZnO/Polyimide Substrates. *J. Mater. Chem. C* **2013**, *1*, 6210-6215.
- [26] Jin, H.; Zhou, J.; He, X.; Wang, W.; Guo, H.; Dong, S.; Wang, D.; Xu, Y.; Geng, J.; Luo, J. K.; Milne, W. I. Flexible Surface Acoustic Wave Resonators Built on Disposable Plastic Film for Electronics and Lab-on-a-Chip Applications. *Sci. Rep.* **2013**, *3*, 2140.
- [27] Zhang, Q.; Wang, Y.; Tao, R.; Torun, H.; Xie, J.; Li, Y.; Fu, C.; Luo, J.; Wu, Q.; Ng, W. P.; Binns, R.; Fu, Y. Q. Flexible ZnO Thin Film Acoustic Wave Device for Gas Flow Rate Measurement. *J. Micromech. Microeng.* **2020**, *30*, 095010.
- [28] Tao, X.; Jin, H.; Mintken, M.; Wolff, N.; Wang, Y.; Tao, R.; Li, Y.; Torun, H.; Xie, J.; Luo, J.; Zhou, J.; Wu, Q.; Dong, S.; Luo, J.; Kienle, L.; Adelung, R.; Mishra, Y. K.; Fu, Y. Q. Three-Dimensional Tetrapodal ZnO Microstructured Network Based Flexible Surface Acoustic Wave Device for Ultraviolet and Respiration Monitoring Applications. *ACS Appl. Nano Mater.* **2020**, *3*, 1468-1478.
- [29] Saifaldeen, Z. S.; Khedir, K. R.; Cansizoglu, M. F.; Demirkan, T.; Karabacak, T. Superamphiphobic Aluminum Alloy Surfaces with Micro and Nanoscale Hierarchical Roughness Produced by a Simple and Environmentally Friendly Technique. *J. Mater. Sci.* **2014**, *49*, 1839-1853.
- [30] Liu, Y.; Li, Y.; el-Hady, A. M.; Zhao, C.; Du, J. F.; Liu, Y.; Fu, Y. Q. Flexible and Bendable Acoustofluidics Based on ZnO Film Coated Aluminium Foil. *Sensors Actuators B* **2015**, *221*, 230-235.
- [31] Liang, W.; Lindner, G. Investigations of Droplet Movement Excited by Lamb Waves on a Non-Piezoelectric Substrate. *J. Appl. Phys.* **2013**, *114*, 44501.
- [32] Smith, W. R.; Gerard, H. M.; Collins, J. H.; Reeder, T. M.; Shaw, H. J. Analysis of Interdigital Surface Wave Transducers by Use of an Equivalent Circuit Model. *IEEE Trans. Microw. Theory Tech.* **1969**, *17*, 856-864.

- [33] Hines, J. H.; Malocha, D. C. A simple transducer equivalent circuit parameter extraction technique. In *Proc. IEEE Ultrason. Symp.* **2003**, 173-177.
- [34] Elmazria, O.; Mortet, V.; El Hakiki, M.; Nesladek, M.; Alnot, P. High velocity SAW using aluminum nitride film on unpolished nucleation side of free-standing CVD diamond. *IEEE Trans. Ultrason. Ferroelect. Freq. Contr.* **2003**, 50, 710-715.
- [35] Shirtcliffe, N. J.; McHale, G.; Atherton, S.; Newton, M. I. An Introduction to Superhydrophobicity. *Adv. Colloid Interface Sci.* **2010**, 161, 124-138.
- [36] Wang, Y.; Zhang, Q.; Tao, R.; Chen, D.; Xie, J.; Torun, H.; Dodd, L. E.; Luo, J.; Fu, C.; Vernon, J.; Canyelles-Pericas, P.; Binns R.; Fu, Y. A rapid and controllable acoustothermal microheater using thin film surface acoustic waves. *Sensors Actuators A* **2021**, 318, 112508.
- [37] Rokhlin, S. I.; Wang, L. Stable Recursive Algorithm for Elastic Wave Propagation in Layered Anisotropic Media: Stiffness Matrix Method. *J. Acoust. Soc. Am.* **2002**, 112, 822-834.
- [38] Lubliner, J. *Plasticity Theory*; Courier Corporation, **2008**.
- [39] Zhang, Q.; Wang, Y.; Li, D.; Yang, X.; Xie, J.; Fu, Y. Bending Behaviors of Flexible Acoustic Wave Devices Under Non-uniform Elasto-plastic Deformation. *Appl. Phys. Lett.* **2021** 118, 121601.
- [40] Arzt, R. M.; Salzmann, E.; Dransfeld, K. Elastic Surface Waves in Quartz at 316 MHz. *Appl. Phys. Lett.* **1967**, 10, 165-167.
- [41] Guo, Y. J.; Lv, H. B.; Li, Y. F.; He, X. L.; Zhou, J.; Luo, J. K.; Zu, X. T.; Walton, A. J.; Fu, Y. Q. High Frequency Microfluidic Performance of LiNbO<sub>3</sub> and ZnO Surface Acoustic Wave Devices. *J. Appl. Phys.* **2014**, 116, 024501.
- [42] Janardan, N.; Panchagnula, M. V. Effect of the Initial Conditions on the Onset of Motion in Sessile Drops on Tilted Plates. *Colloids Surf. A: Physicochem. Eng. Aspects* **2014**, 456, 238-245.
- [43] Bussonnière, A.; Baudoin, M.; Brunet, P.; Matar, O. B. Dynamics of Sessile and Pendant Drops Excited by Surface Acoustic Waves: Gravity Effects and Correlation between Oscillatory and Translational Motions. *Phys. Rev. E* **2016**, 93, 053106.

## Table of Contents

